Characterization of iron oxide thin film prepared by the sol–gel method

N. TAKAHASHI, N. KAKUTA, A. UENO, K. YAMAGUCHI*, T. FUJII*
*Department of Materials Science and *Department of Electrical and Electronic Engineering, Toyohashi University of Technology, Tempaku, Toyohashi, Aichi 440, Japan.*

T. MIZUSHIMA, Y. UDAGAWA
Institute for Molecular Science, Myodaiji, Okazaki, Aichi 444, Japan

Thin films consisting of γ-Fe_2O_3 particles were prepared by a spin-on process using a solution of iron(III) nitrate dissolved in ethylene glycol. Film thickness was observed to be controlled by the solution viscosity as well as the revolution of a spinner. Local structures around iron ions in the solution were studied by extended X-ray absorption fine structure spectroscopy and the formation of an $(FeO_x)_n$ cluster was deduced. A film thus prepared was confirmed to consist of finely divided γ-Fe_2O_3 particles by TEM observation. Magnetic and optical properties of the films are briefly discussed.

1. Introduction

Aiming at the discovery of novel properties of a solid surface, extensive studies have been reported on the preparation and characterization of solid thin films. In most of the studies the films were prepared by dry methods such as the evaporation of metals *in vacuo* [1–4], sputtering with ionized inactive gases [5–8] and chemical vapour deposition [9–12]. Although these dry methods are preferred for the production of ultra-thin films, < 10 nm, wet methods, such as dipping a substrate into solutions containing metal ions [13–15] and a spin-on process [16, 17] have often been employed for the preparation of thin films with submicrometre thickness.

A wet method using sol or gel suspension solutions was first reported by Schroder [18], and further developed by Dislich [19–21], Sakka [22, 23] and Yoldas [24, 25] with their colleagues for the production of silica, barium titanate and alumina thin films, respectively. Recently, the preparation and characterization of iron oxide thin films has been carried out by dipping a glass plate in sol or gel solutions containing iron ions [26, 27], but as yet the techniques to control the film thickness have not been developed.

In the present work iron oxide thin films consisting of fine maghaemite (γ-Fe_2O_3) particles were prepared by spin coating a gel suspension consisting of iron ions and ethylene glycol oligomers. The film thickness was prone to be controlled by the viscosity of the suspension solution as well as the spinning revolution. Local structure around the iron ions in the gel suspension was monitored by extended X-ray absorption fine structure (EXAFS) spectroscopy to deduce the mechanism of the formation of finely divided maghaemite particles, that is, the constituent of iron oxide thin films [28].

2. Experimental procedure

2.1. Preparation of thin films

The films employed in this work were prepared by spin coating a gel solution of iron(III) nitrate dissolved in ethylene glycol. The gel was prepared in a three-port flask by stirring the solution at 80 °C in flowing nitrogen. With stirring time, the viscosity of the solution increased, measured at 25 °C by a rotating viscometer (Tokyo Seiki Co., Visconic E.L.D.). The concentration of $Fe(NO_3)_3 \cdot 9H_2O$ in the solution was kept to 15 wt % in all experiments.

A few droplets of the gel solution were poured over a glass plate (38 mm × 26 mm × 1 mm), spinning at the correct rate under infrared light irradiation to heat the glass plate during spinning. The spinning revolution could be varied from 1400 to 4000 r.p.m. and spinning was carried out for 10 min in each run. The glass plate thus coated was dried in an oven at 110 °C for 15 min, followed by calcination in air at various temperatures for 5 h.

2.2. SEM and TEM observation

The calcined sample was submitted to SEM (scanning electron microscope, Hitachi, Model 650-X) with a magnification of × 4000 under an accelerating voltage of 15 kV. A part of the calcined films was removed from the glass plate and suspended in ethanol with the aid of a supersonication. Some of the finest part of the suspension was pipetted on to a microgrid for TEM (transmission electron microscope, Hitachi Model H-800), operated at an accelerating voltage of 200 kV with a magnification of × 10⁵.

2.3. Measurement of film thickness

Some of the films were submitted to a surface roughness tester (Nihon Shinkugijutsu Co., DEKTAK),

equipped with a diamond probe. On the basis of the thickness thus obtained, the thicknesses of the other films were calculated from the transmission of visible light ($\lambda = 510$ nm) through the films using Lambert–Beer's law. All the samples employed for thickness measurements were calcined at 450 °C for 5 h.

2.4. EXAFS measurements

A small amount of the gel solution was placed between two sheets of organic thin films and subjected to EXAFS measurements. The EXAFS spectrometer employed consists of a rotating anode X-ray generator (Rigaku RU-200), a Johansson cut and bent LiF(2 2 0) crystal and a solid state detector. In the analysis of the EXAFS spectra, the oscillatory part was subtracted and was converted to k space and Fourier transformed by the standard procedures [29, 30]. The least-squares curve fitting with the back-transformed oscillation in k space was performed using Teo and Lee's parameters, with the formula derived from single-scattering theories [31, 32].

2.5. Magnetic properties of films

Magnetization and coercive force of the films calcined at various temperatures were measured by a vibrating sample magnetometer (Toei Kogyo Co., VSM-2) with 80 Hz vibrating frequency and a magnetic field up to 2 T. All the measurements were carried out at room temperature. Note that magnetization of the glass plate (diamagnetic) was small enough to be ignored in the present work.

2.6. Optical properties of films

The transmissions of near infrared and visible lights through the films calcined at various temperatures were measured in the wavelength ranging from 300 to 2000 nm at room temperature (Hitachi, Monochromater 330).

2.7. X-ray diffraction measurements

X-ray diffraction patterns of the dried and calcined films were measured by a diffractometer (Rigaku, Geigerflex), operated at 30 kV with a filament current of 15 mA using a nickel filter for $CuK\alpha$ radiation.

2.8. Surface area of films

The surface area of the films calcined at 450 °C for 5 h was measured by BET method using nitrogen at its liquid temperature and was compared with the surface area of iron oxide powders prepared by evaporation and pyrolysis of the gel solution at 450 °C.

3. Results

3.1. Change in viscosity of solution

Increase in the viscosity of the solution of iron nitrate(III) dissolved in ethylene glycol at 80 °C with the stirring time is shown in Fig. 1, the concentration of iron nitrate being 15 wt %. The viscosity was measured at 25 °C by pipetting a small amount of the sample solution at 80 °C into a glass vial to be rapidly cooled to 25 °C. The accuracy of temperatures during the viscosity measurements is guaranteed within ± 0.5 °C.

3.2. Control of film thickness

Fig. 2 shows the thickness of films prepared by a solution containing 15 wt % iron nitrate with the viscosity of a gel solution. The film thickness was found to increase with increase in the viscosity but decrease with increasing spinner revolution. Arrowed marks in Fig. 2 indicate that the thickness was measured by a surface roughness tester.

3.3. SEM and TEM observations

A scanning electron micrograph of a typical film calcined at 450 °C for 5 h (85 nm thick) is given in Fig. 3, indicating almost homogeneous surface structure in all parts of the film, though a few small holes and cracks were still observed. Fig. 4 shows a transmission electron micrograph of the film, 85 nm thick. It was found that the film is composed of finely divided spherical particles. It should be mentioned that the mean particle size in the film is estimated to be 100 nm, being very close to the film thickness, 85 nm.

3.4. EXAFS analysis

Figs 5 and 6 show the changes in the Fourier transforms of the EXAFS as the reaction proceeds, as well as an EXAFS spectrum of the gel solution (formed after stirring for 10 h) and the associated Fourier transform. The inverse Fourier transform of the second peak in Fig. 6 and the best-fit curve assuming Fe–O–Fe and Fe–O–C structures are given in Fig. 7, where the nearest coordination number of the iron atom around the central absorbing atom (N), the interatomic distance (R), Debye–Waller factor (σ) were determined to be 4, 0.307 nm, and 0.0081 nm respectively, by assuming the mean free path of photoelectron (λ) to be 0.6 nm.

3.5. Magnetic properties of the films

Magnetization curves of the films calcined at 350, 400, 450 and 500 °C for 5 h are shown in Fig. 8a to d, respectively. The film thickness is estimated to be 85 nm, as mentioned above, when calcined at 450 °C for 5 h. The temperature dependence of the saturation magnetization of films is given in Fig. 9. The highest coercive force observed was around 250 Oe*, being achieved for the films calcined at 450 °C. The saturation magnetization increased gradually on increasing the calcination temperature to 450 °C and then decreased at temperatures higher than 500 °C.

* $1 \text{ Oe} = \frac{1}{4}\pi \times 10^3 \text{ A m}^{-1}$.
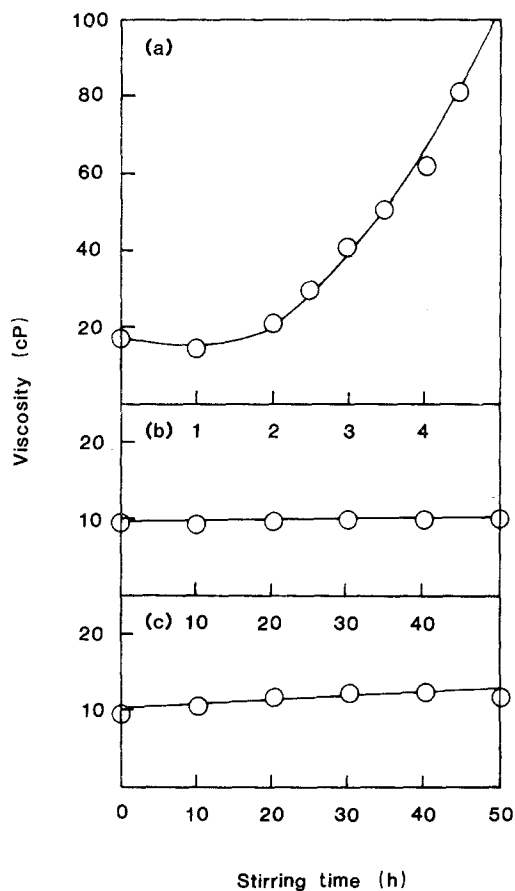
Figure 1 Change in the viscosity of ethylene glycol solution containing 15 wt % of (a) iron(III), (b) nickel(II), and (c) cobalt(III) nitrates with the stirring time at 80 °C; the viscosities were measured at 25 °C.

Figure 2 Change in the thickness of films calcined at 450 °C with the viscosity of solution and the spinning rate; arrows indicate that the thickness was measured with a surface roughness tester.

here. The shift of the absorption edge with the calcination temperature is depicted in Fig. 11.

3.6. Optical properties of films

Absorption spectra of films dried at 110 °C and calcined at various temperatures are shown in Fig. 10, where higher than 90% transmittance in the near-infrared region is observed for all the films employed

3.7. XRD measurements

XRD patterns of the films calcined at 350, 400, 450 and 500 °C are given in Fig. 12a to d, respectively. No diffraction peaks were observed for the films calcined at temperatures lower than 450 °C, indicating the presence of amorphous or finely divided γ-Fe_2O_3 particles in these films, while for the films calcined at 500 °C, a tiny diffraction peak due to α-Fe_2O_3 was confirmed, suggesting that the phase transition of γ-Fe_2O_3 to α-Fe_2O_3 occurred around 500 °C.
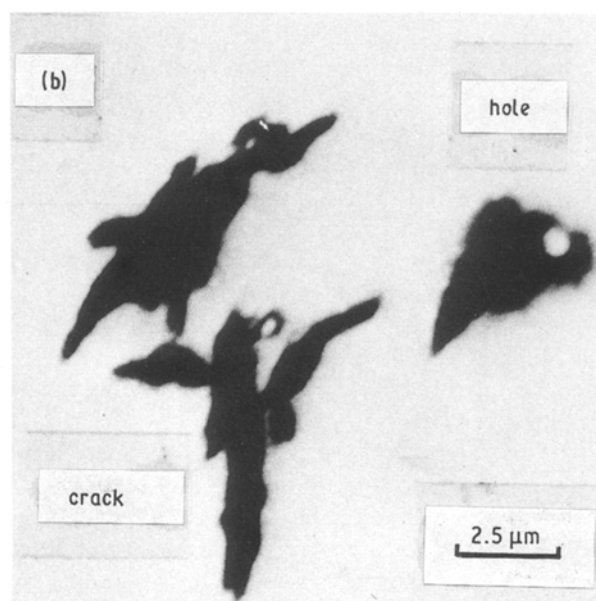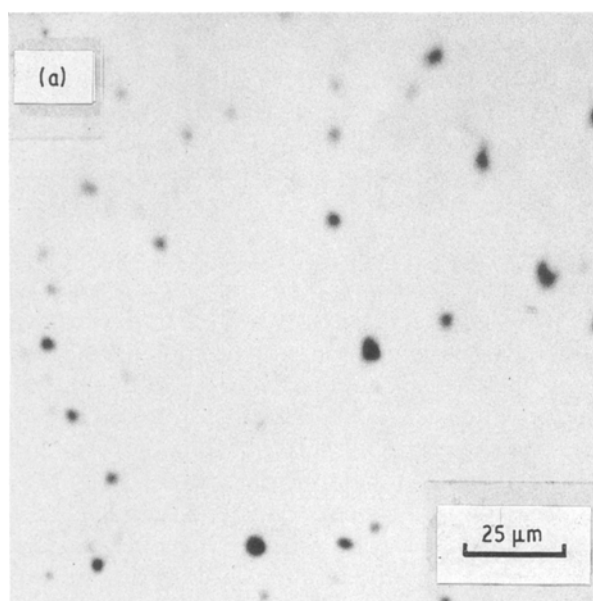
Figure 3 Scanning electron micrographs of the film calcined at 450 °C. The film (85 nm thick) was prepared from a gel solution with a viscosity of 50 cP at 25 °C.

499
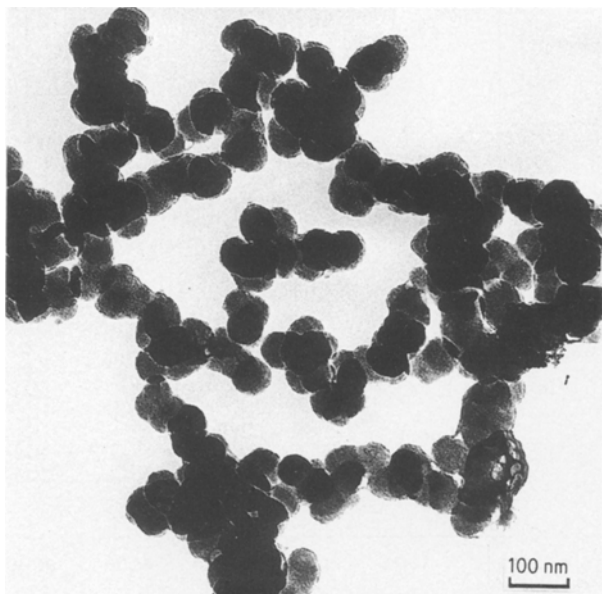
Figure 4 Transmission electron micrographs of γ-Fe$_2$O$_3$ particles, i.e. constituents of films with 85 nm thickness. Films were prepared from the gel solution with a viscosity of 50 cP and calcined at 450 °C for 5 h.

3.8. Surface area of films

Table I summarizes the BET surface areas of the 85 nm thick calcined films and of iron oxide powders prepared from the gel solution by vacuum evaporation and calcination at 450 °C for 5 h. The large surface area of the calcined films was confirmed.

4. Discussion

During stirring the solution of Fe(III) nitrate dissolved in ethylene glycol at 80 °C, the viscosity of the solution increased. The increase in viscosities of the solutions of nickel and/or cobalt nitrates dissolved in ethylene glycol was not observed even after prolonged stirring for 70 h, as shown in Fig. 1 for comparison. This suggests that Fe(III) ions are effective catalysts for the polymerization of ethylene glycol. Because the local structures around Fe(III) ions in the solution are of fundamental importance to the understanding of the reaction, EXAFS measurements were carried out. Only one peak which should be assigned to the Fe–O bond is observed in the Fourier transform of the EXAFS of Fe(III) nitrate immediately after the dissolution in ethylene glycol at 80 °C. As the reaction proceeds by stirring, a second peak shows up and gradually increases in intensity, as shown in Fig. 5. Two models for the reaction can be conceived; one is that the Fe(III) ions are not only catalysts but also reactants to react with ethylene glycol, leading to the formation of –Fe–O–C– structures. The other is that Fe(III) ions are merely the catalysts of ethylene glycol polymerization and some of the iron ions are enclosed by the resulting polymer chains, followed by aggregation of the iron ions, probably being hydrated ions. Hence, the local structures around the iron atoms are expected to be –Fe–O–Fe– in this model. To determine which is the case, a least-squares fit calculation was attempted to obtain the best-fit curve to the
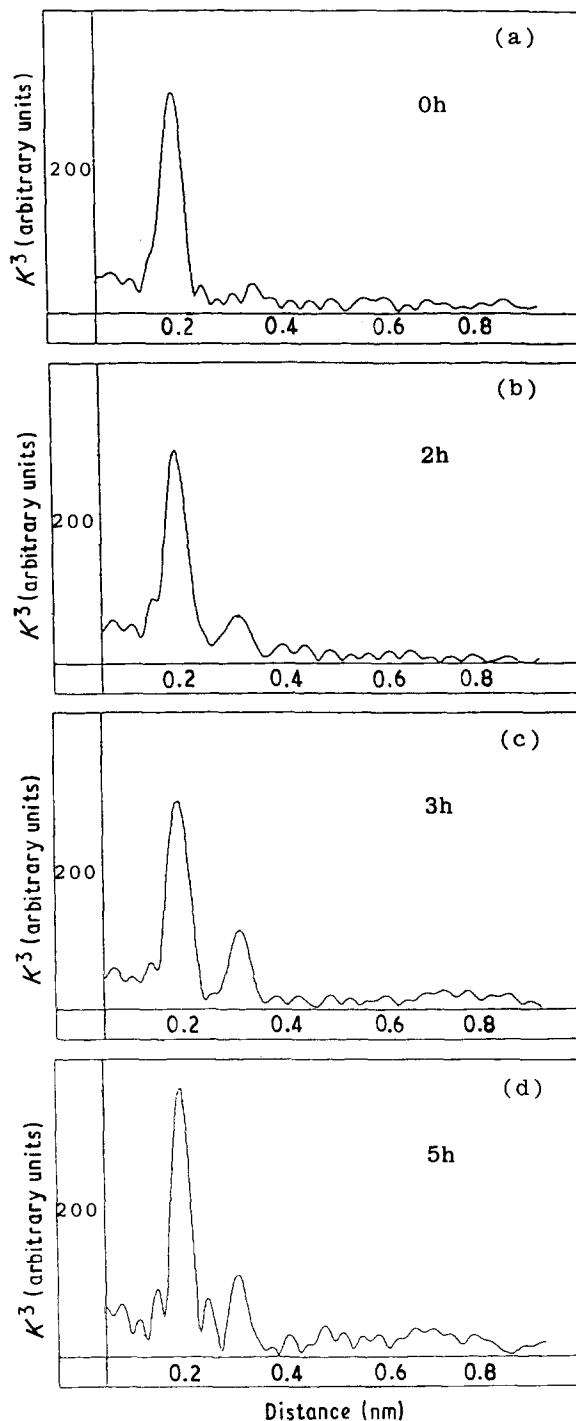
Figure 5 Change in the Fourier transforms of EXAFS of the solution with stirring time at 80 °C. (a) Immediately after dissolution of iron nitrate, and after stirring for (b) 2 h, (c) 3 h and (d) 5 h.

inverse Fourier transform of the second peak in Fig. 6 by assuming carbon or iron as a back-scatterer. It is evident that the calculation for Fe–O–Fe structure confirms the observation, but that for the Fe–O–C structure does not, as shown in Fig. 7. Consequently, the formation of (FeO$_x$)$_n$ clusters surrounded by polymer chains is expected during stirring of the solution of iron(III) nitrate dissolved in ethylene glycol. Many of these clusters further coagulate to form finely divided iron oxide particles when the films were calcined. The reasons why the resultant iron oxides are maghaemite are, however, still ambiguous, though we have already reported the formation of tiny maghaemites as the precursors of iron metal particles in Fe/SiO$_2$
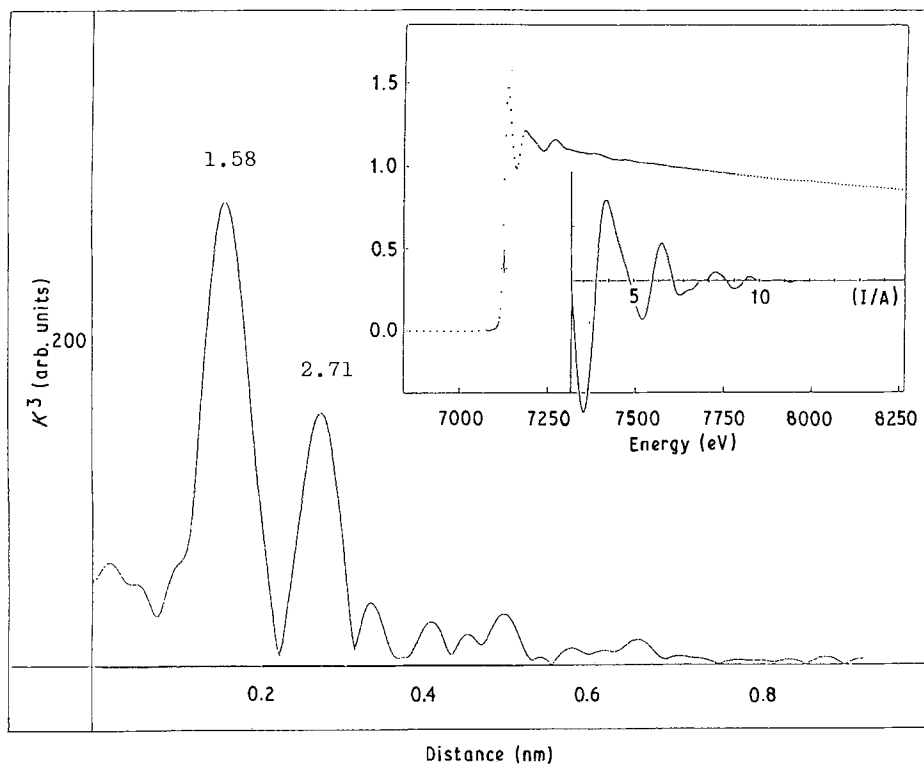
Figure 6 EXAFS spectrum and the associated Fourier transform of the gel solution, formed after stirring for 10 h.
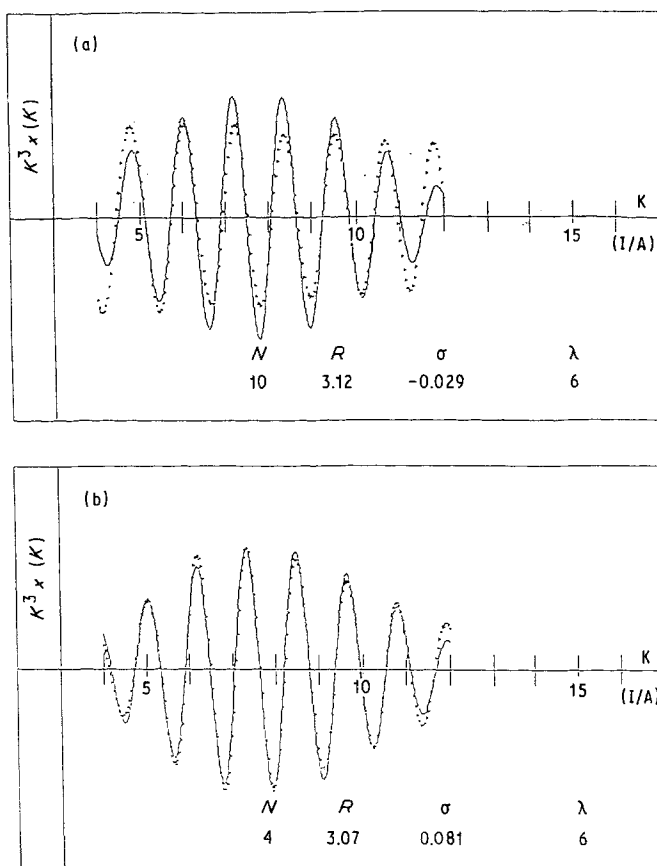
Figure 7 Inverse Fourier transform (———) of the second peak in Fig. 6, and the least-squares fit calculation (- - - -) assuming (a) Fe–O–C and (b) Fe–O–Fe structures, respectively.

catalyst prepared by hydrolysis of the mixed solution of iron(III) nitrate in ethylene glycol and tetraethoxysilane [33].

The films prepared are of consistent thickness with the viscosities of the gel solutions and with the spinning revolutions, as is given in Fig. 2. The relationship between film thickness, viscosity of the solution and

the rate of raising the glass plate from the solution has been established for the production of thin films by dipping methods [34, 35]; $t = K(\eta v/\rho g)$, where ρ and η are the density and viscosity of solution, respectively, v is the rate of raising the glass plate and g is the acceleration of gravity. Thus, the film thickness increases with increasing the raising rate of the glass as
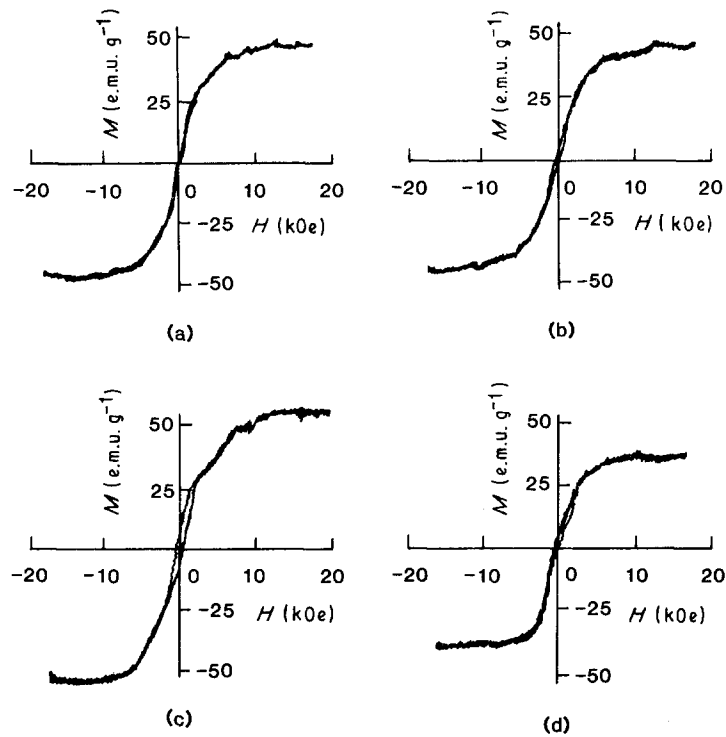
Figure 8 Magnetization curves of films calcined at (a) 350 °C, (b) 400 °C, (c) 450 °C and (d) 500 °C for 5 h, respectively. Films were prepared in a similar manner to that mentioned in Fig. 4.
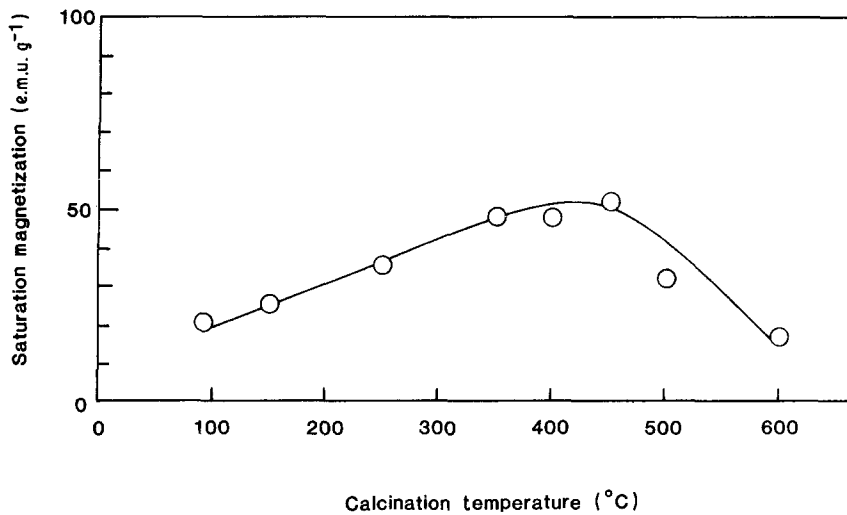
Figure 9 Dependence of calcination temperature on the saturation magnetization of films depicted in Fig. 8.

Figure 10 Absorption spectra of the film dried at (a) 110 °C, and of the films calcined at (b) 350 °C and (c) 500 °C for 5 h, respectively. Films were prepared in a similar way to that mentioned in Fig. 4.

502
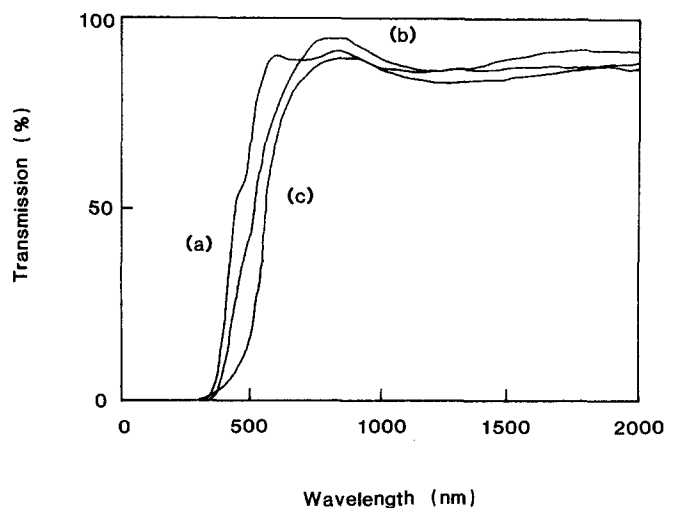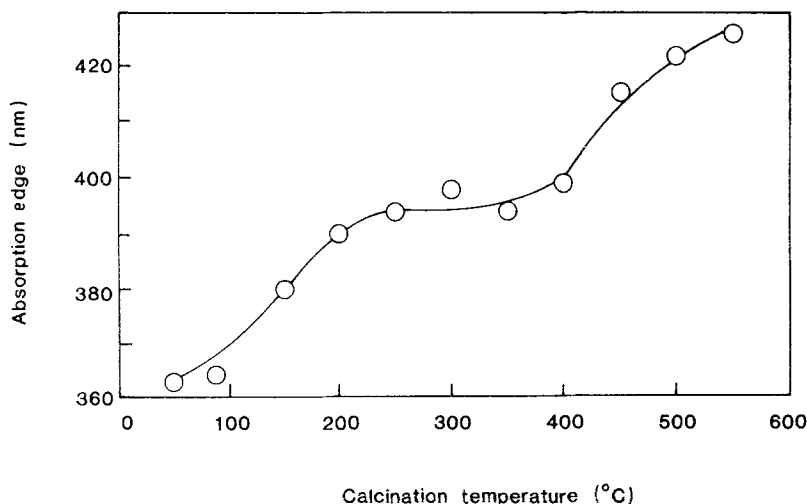
Figure 11 Shift of the absorption edge with calcination temperatures estimated from the spectra shown in Fig. 8.

Absorption edge (nm) vs Calcination temperature (°C)
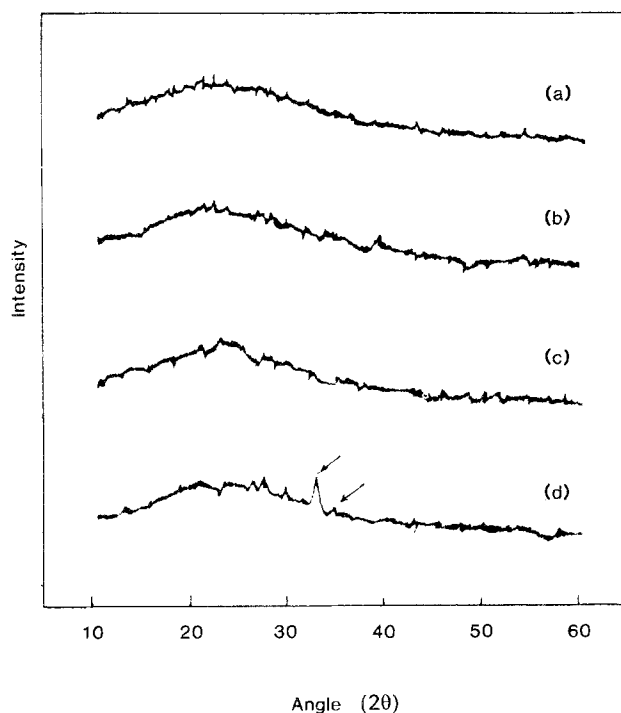
Figure 12 XRD spectra of the films calcined at (a) 350 °C, (b) 400 °C, (c) 450 °C and (d) 500 °C, respectively; the films were prepared in a similar manner to that mentioned in Fig. 4, and the arrows in the figure indicate the diffraction peaks due to α-Fe_2O_3.

Intensity vs Angle (2θ)

TABLE I BET surface areas of the film (85 nm thick) shown in Fig. 3 and of the iron oxide powder; the preparation conditions of the iron oxide powder are given in the text

	γ-Fe_2O_3 film	γ-Fe_2O_3 powder
BET surface area (m^2 g^{-1})	80	25

well as the viscosity of the solution. On the analogy of the dipping methods, the raising rate is expected to be substituted by the spinning revolution in a spin-on process. This however, was not the case because the film thickness was observed to increase with decreasing spinner revolutions (see Fig. 2). Thus, the raising rate and the spinner revolution have an opposite effect

on the control of film thickness. In the present work, the thickness of iron oxide films was proved to be controlled in the range between 30 and 300 nm.

Although the holes and cracks on the films are emphasized in the scanning electron micrograph (Fig. 3), the surface of the present films is so smooth and fewer holes and cracks on the films were detected. A transmission electron micrograph, shown in Fig. 4, is evidence that the film is composed of finely divided iron oxide particles with a homogeneous size; 100 nm. Because the thickness of the film used in the TEM observation was estimated to be around 85 nm, nearly equal to the particle size, it might be possible to say that some parts of the film consist of single-layer dispersion of the iron oxide particles. The uniform size of the particles is attributed to the homogeneous dispersion of $(FeO_x)_n$ clusters in the solution. As can be seen in Table I, the specific surface area of the iron oxide particles is as large as 80 m^2 g^{-1}, measured by removing the films from the glass plates. The mean particle size of iron oxide is estimated to be 100 nm and the density of γ-Fe_2O_3 is 5.15 g cm^{-3}, hence, the specific surface area can be calculated assuming that the particles are quite smooth spheres; $S = 6/\rho d$, where ρ and d are the density of γ-Fe_2O_3 and the diameters of the spherical particles, respectively. The calculated surface area is 11.7 m^2 g^{-1}, much less than that observed (80 m^2 g^{-1}). This means that the iron oxide particles, which construct the films, are rather porous spheres. The iron oxide particles constituting the film are finely divided spheres, resulting in no structural magnetic anisotropy.

The magnetization curves of the film calcined at various temperatures are given in Fig. 8, indicating the lowest coercive force of all the films employed, though the maximum of 250 Oe was measured for the films calcined at 450 and 500 °C. At present, the films prepared here would not be available for practical use as magnetic memories because of such low coercive forces [36, 37], while the saturation magnetization of the film increased with increasing calcination temperature, up to 450 °C, where 52 e.m.u./g Fe_2O_3 was obtained. Because the saturation magnetization of bulk γ-Fe_2O_3 is $\sim$75 e.m.u g^{-1}, the fraction of γ-Fe_2O_3 species in the film was calculated to be 70%.

Increase in the saturation magnetization with increasing calcination temperature is elucidated in terms of the growth of tiny γ-Fe_2O_3 particles, and the decrease on calcination at 500 °C (Fig. 9) is ascribed to the phase transition of γ-Fe_2O_3 to α-Fe_2O_3 (haematite) [38, 39]. Evidence for this phase transition was obtained by X-ray diffraction measurements, as shown in Fig. 12, where the diffraction peak assigned to α-Fe_2O_3 was observed for the films calcined at 500 °C. For the films calcined at temperatures lower than 450 °C, no diffraction peaks were observed, suggesting that the fine maghaemite particles observed by SEM will be coagulated by much smaller crystallites of maghaemite. These are too small to be detected by X-ray diffraction measurements.

Higher than 90% transmittance of near-infrared light was obtained for the present films (see Fig. 10). The high transparencies of the present films originated from the high qualities, such as fewer vacancies (holes and cracks) in the films and homogeneous dispersion of finely divided maghaemite particles. Because γ-Fe_2O_3 has a considerably large magneto-optical Faraday effect ($\theta_F = -2.2 \times 10^4$ deg cm^{-1} at $\lambda = 442$ nm) [40, 41], the films prepared could be used as a magneto-optical recording medium, if their coercive forces are improved to some extent. Shifts of the absorption edge to higher wavelength with the calcining temperature are shown in Fig. 11. For the dried films the absorption edge was observed to be 365 nm and shifted to 395 nm with increasing calcination temperature up to 200 °C, being ascribed to the evaporation of ethylene glycol remaining in the dried films. It should be noted that the boiling point of ethylene glycol is 198 °C. A constant wavelength of the adsorption edge was observed for films calcined at temperatures from 200 to 400 °C. Shifts of the absorption edge were again observed when the films were calcined at temperatures higher than 450 °C, probably because of the formation of α-Fe_2O_3 in the films.

5. Conclusions

1. Thin iron oxide films, mainly composed of finely divided γ-Fe_2O_3 particles, were simply prepared by spin coating the gel solution of iron(III) nitrate dissolved in ethylene glycol.

2. Local structure around iron(III) ions in the gel solution was proved to be $(FeO_x)_n$ clusters by EXAFS measurements.

3. Iron oxides in the films were spherical particles, leading to no structural magnetic anisotropy. Thus, the coercive forces observed for the present films were poor.

4. The films were found to be transparent for near-infrared, suggesting fewer vacancies and a high dispersion of iron oxides in the present films.

References

1. G. BATE, *IEEE Trans. Magn. Mag-1* **3** (1965) 193.
2. T. YAO and S. MAEKAWA, *J. Crystal Growth* **53** (1981) 432.
3. P. M. PARK, H. A. MAR and N. M. SALANSKY, *J. Vac. Sci. Technol.* **B3** (1985) 676.
4. S. P. PARKIN, V. Y. LEE, A. I. NAZAL, R. SAVOY, T. C. HUANG, G. GORMAN, and R. BEYERS, *Phys. Rev. B* **38** (1988) 6531.
5. J. K. LIN, M. SIVERTSEN and J. H. JUDY, *J. Appl. Phys.* **57** (1985) 4000.
6. C. HWANG, M. M. CHEN and G. CASTILLO, *J. Appl. Phys.* **63** (1988) 3272.
7. M. NAKAO, R. YUASA, M. NEMOTO, H. KUWAHARA, H. MUKAIDA and A. MIZUKAMI, *Jpn J. Appl. Phys.* **27** (1988) L849.
8. J. TAMAKI, S. NAKAYAMA, M. YAMAMURA and T. IMANAKA, *J. Mater. Sci.* **24** (1989) 1582.
9. R. D. DUPIS and P. D. DUPKUS, *Appl. Phys. Lett.* **31** (1977) 466.
10. H. ABE, T. NAKAMORI, T. KANAMORI and S. SHIBATA, *J. Crystal Growth* **93** (1988) 929.
11. H. YAMANE, H. KUROSAWA, T. HIRAI, H. IWASAKI, N. KOBAYASHI and Y. MOTO, *Jpn J. Appl. Phys.* **27** (1988) L1495.
12. M. LANGLET and J. C. JOUBERT, *J. Appl. Phys.* **64** (1988) 780.
13. H. DISLICH and P. HINZ, *J. Non-Cryst. Solids* **48** (1982) 11.
14. G. KORDAS, R. A. WEEKS and N. ARFSTEN, *J. Appl. Phys.* **57** (1985) 3812.
15. K. C. CHEN, A. JANAH and J. D. MACKENZIE, *ibid.* **73** (1986) 731.
16. K. OGISU and S. TAKAHASI, *IEEE Trans. Mag.* **Mag.-21** (1985) 1489.
17. M. KUISL, *Thin Solid Films* **157** (1988) 129.
18. H. SCHRÖDER, "Physics of Thin Films", Vol. 5, edited by G. Hass and R. E. Thun (Academic Press, New York, 1964) p. 87.
19. H. DISLICH, *Angew. Chem. Int. Ed. Engl.* **10** (1971) 363.
20. *Idem, J. Non-Cryst. Solids* **73** (1985) 599.
21. *Idem, Thin Solid Films* **77** (1981) 129.
22. S. SAKKA, "Treatise on Materials Science and Technology", Vol. 22 "Glass III", edited by M. Tomozawa and R. Doremus (Academic Press, New York, 1982) p. 129.
23. *Idem, J. Non-Cryst. Solids* **48** (1982) 1.
24. B. E. YOLDAS, *Ceram. Bull.* **54** (1975) 289.
25. *Idem, Amer. Ceram. Soc. Bull.* **54** (1975) 286.
26. G. KORDAS, *Mater. Res. Soc. Symp. Proc.* **73** (1986) 685.
27. K. TANAKA, T. YOKO, M. ATARASHI and K. KAMIYA, *J. Mater. Sci. Lett.* **8** (1989) 83.
28. K. TOHJI, Y. UDAGAWA, T. KAWASAKI and K. MASUDA, *Rev. Sci. Instrum.* **54** (1983) 1482.
29. K. TOHJI, Y. UDAGAWA, S. TANABE, T. IDA and A. UENO, *J. Amer. Chem. Soc.* **106** (1984) 5172.
30. K. TOHJI, Y. UDAGAWA, S. TANABE and A. UENO, *ibid.* **106** (1984) 612.
31. D. SAYERS, E. A. STERN and F. W. LYTLE, *Phys. Rev. Lett.* **27** (1971) 1204.
32. E. A. STERN, *Phys. Rev. B* **10** (1974) 3027.
33. T. IDA, H. TSUIKI and A. UENO, *J. Catal.* **106** (1987) 428.
34. L. D. LANDAU and V. G. LEVICH, *Acta Physica Chim. URSS* **17** (1942) 41.
35. C. C. YANG, J. Y. JOSEFOWICZ and L. ALEXANDRU, *Thin Solid Films* **74** (1980) 117.
36. S. CHIKAZUMI (ed.) "Handbook of Magnetic Compound" (Asakura-Shoten, Tokyo, 1975) p. 616 (in Japanese).
37. R. L. COMSTOCK and E. B. MOORE, *IBM J. Res. Develop.* Nov. (1974) 556.
38. F. E. DEBOER and P. W. SELWOOD, *J. Amer. Chem. Soc.* **76** (1954) 3365.
39. S. MÖRUP and H. TOPSØE, *Appl. Phys.* **11** (1976) 63.
40. H. WANG, J. SHEN and J. QIAN, *J. Mag. Magn. Mater.* **73** (1988) 103.
41. N. F. BORRELLI, S. L. CHEN and J. A. MURPHY, *IEEE Trans. Magn.* **Mag-8** (1972) 648.